BNL-103690-2014-TECH

AGS/RHIC/SN 065;BNL-103690-2014-IR

Data Analysis of the Magnetic Field Measurement of a Helical Dipole Prototype Magnet by the Rotating Coil

T. Tominaka

September 1997

Collider Accelerator Department

Brookhaven National Laboratory

U.S. Department of Energy

USDOE Office of Science (SC)

DISCLAIMER

Alternating Gradient Synchrotron Department
Relativistic Heavy Ion Collider Project
BROOKHAVEN NATIONAL LABORATORY
Upton, New York 11973

Spin Note

AGS/RHIC/SN No. 065

Data Analysis of the Magnetic Field Measurement of a Helical Dipole Prototype Magnet by the Rotating Coil

T. Tominaka (RIKEN, Japan)

AGS Department, Brookhaven National Laboratory, NY 11973

September 22, 1997

DATA ANALYSIS OF THE MAGNETIC FIELD MEASUREMENT OF A HELICAL DIPOLE PROTOTYPE MAGNET BY THE ROTATING COIL

T. Tominaka (RIKEN, Japan)

September 22, 1997

1 INTRODUCTION

The data analysis of the magnetic field measurement is made to obtain the multipole contents of the helical dipole prototype magnet.[1,2,3]

2 PARAMETERS OF THE PICK-UP COILS

The magnetic field at the middle portion of the half-length helical dipole prototype was measured, using the following 5 windings. [1,2] The parameters of 5 windings, dipole #1, dipole #2, tangential, quadrupole #1, and quadrupole #2, which are used for the data analysis, are listed in Table 1. The other parameters of 5 windings are neglected on this data analysis.[1] The radii of these pick-up coils are about 27 mm, whereas the reference radius on which the components have to be estimated is $r_0 = 31$ mm. Therefore, it results to extrapolate the measured values to the larger reference radius.

Table 1 Parameters of 5 windings, dipole #1, dipole #2, tangential, quadrupole #1, and quadrupole #2, used for the data analysis

	Dipole #1	Dipole #2	Tangential	Quad #1	Quad #2
Number of turns : N	3	3	30	3	3
Length : Δz (mm)	229.718	230.263	229.870	229.718	229.718
Radius : r_c (mm)	27.4315	27.4099	27.4110	27.4422	27.4621
Nominal opening angle (deg)	180.000	180.000	15.000	90.000	90.000

3 DATA ANALYSIS OF THE RESULTS MEASURED BY PICK-UP COILS

3.1 Method of Data Analysis

On the magnetic measurement, the integration time, Δt, and the voltage, V for each winding were measured at 128 rotational steps per one revolution. On this data analysis, it is postulated that the angular interval between each measurement step is $2\pi/128$ (= constant), whereas the rotational speed is not constant. According to the following steps, the data analysis is made.

1) From both of the voltage, V(i), (i = 1, 2, ... , 128), and the integration time, $\Delta t(i)$, measured at each step, the magnetic flux, $\Phi(k)$, at the step, #k, corresponding angle $\theta_k = (2\pi/128) \times k$, is calculated as follows,

$$\Phi(\theta_k) = \Phi(\frac{2\pi}{128} k) = \sum_{i=1}^{k} \Delta\Phi(i) = \sum_{i=1}^{k} V(i) \times \Delta t(i) \quad . \tag{1}$$

Though $\Phi(2\pi) = \Phi(0) = 0$ is required, the following measured value for $\Phi(2\pi)$ is actually obtained at I = 199.98 A,

$$\Phi(2\pi) = \sum_{i=1}^{128} \Delta\Phi(i) = \sum_{i=1}^{128} V(i) \times \Delta t(i) = 3.5 \times 10^{-4}\ \Phi_{p\text{-}p} \quad , \tag{2}$$

where $\Phi_{p\text{-}p}$ is the peak - peak value of $\Phi(\theta)$. It can be considered that this discrepancy is caused by the experimental error. On this data analysis, $\Phi(2\pi)$ is forced to be zero. On this step of the data reduction, the magnetic flux, $\Phi(\theta)$, and the origin of the angle θ of $\Phi(\theta)$ in Eq. (1) are rather arbitrary.

2) The Fourier analysis for the function of $\Phi(\theta)$ in Eq.(1) is made as follows,

$$\Phi(\theta) = \frac{A(0)}{2} + \sum_{n=1}^{\infty} A(n) \cos\left\{n(\theta - \theta_0(n))\right\}. \tag{3}$$

With the introduction of the new angular coordinate with $\theta' = \theta - \theta_0(n=1)$, the following new $\Phi'(\theta')$ is obtained,

$$\Phi'(\theta') = \Phi(\theta' + \theta_0(n)) - \frac{A(0)}{2} = \sum_{n=1}^{\infty} A(n) \cos\left\{n(\theta' + \theta_0(1) - \theta_0(n))\right\}. \tag{4}$$

Finally,

$$\Phi'(\theta') = \sum_{n=1}^{\infty} A(n) \left\{b_n' \cos(n\theta') + a_n' \sin(n\theta')\right\}. \tag{5}$$

can be obtained with $b'_1 = 1$, $a'_1 = 0$.

3) As the last step of the data analysis, the multipole components are calculated from the comparison between Eq. (5) and the expression for the radial magnetic flux enclosed by each pick-up coil, shown in the reference [3]. For example, with respect to the tangential winding, the following expression for the radial magnetic flux of Eq. (15) in the reference [3] is used,

$$\Phi_r(\theta) = B_{ref}(k)\, r_0 \sum_{n=1}^{\infty} n! \left[\frac{2}{n\, k\, r_0}\right]^n \left\{k\, r_c\, I_{n-1}(n\, k\, r_c) - I_n(n\, k\, r_c)\right\} \times$$
$$\sin\left(\frac{n\pi}{24}\right) \frac{4}{k\, n^2} \sin\left(n\, k\, \frac{\Delta z}{2}\right) \left\{b_n(k) \sin\left(n\theta + \frac{n\pi}{2}\right) - a_n(k) \cos\left(n\theta + \frac{n\pi}{2}\right)\right\}, \tag{6}$$

where k is the rate of twist in the body of helical dipole, and the value of $k = 2\pi/2.4$ (rad/m) = 150.0 (deg/m) is adopted for this analysis. The difference of the estimated harmonic contents between k = 150.0 (deg/m) and $k = 2\pi/2.4/(1 - 0.00415)$ (rad/m) = 150.6 (deg/m) with the effect of the expected thermal contraction of Al coil bobbin of 0.415 %, is also checked to be not so large. Then, the reference field, $B_{ref}(k)$ is obtained as follows,

$$B_{ref}(k) = \frac{A(1)}{N\, r_0 \left\{n! \left[\frac{2}{n\, k\, r_0}\right]^n \left\{k\, r_c\, I_{n-1}(n\, k\, r_c) - I_n(n\, k\, r_c)\right\} \sin\left(\frac{n\pi}{24}\right) \frac{4}{k\, n^2} \sin\left(n\, k\, \frac{\Delta z}{2}\right)\right\}_{n=1}}, \tag{7}$$

where N (= 30) is the number of turns of the tangential winding. The helical normal sextupole coefficients $b_3(k)$ is also obtained as follows,

$$b_3(k) = -\frac{A(n=3) \times b_3'}{N\, B_{ref}(k)\, r_0 \left\{n! \left[\frac{2}{n\, k\, r_0}\right]^n \left\{k\, r_c\, I_{n-1}(n\, k\, r_c) - I_n(n\, k\, r_c)\right\} \sin\left(\frac{n\pi}{24}\right) \frac{4}{k\, n^2} \sin\left(n\, k\, \frac{\Delta z}{2}\right)\right\}_{n=3}}. \tag{8}$$

Similarly, other normal and skew multipole coefficients, $b_n(k)$, $a_n(k)$, are calculated.
This method of data reduction is also confirmed with the simulation for the data acquisition at 128 angular points in the helical dipole with the prescribed arbitrary normal and skew multipole coefficients, $b_n(k)$ and $a_n(k)$, as shown in Table 2. In Table 2, both of b_n-spec. and a_n-spec. are the prescribed normal and skew multipole coefficients, whereas both of b_n-f.a. and a_n-f.a. are the resultant multipole coefficients, calculated from the Fourier analysis for the 128 angular points. It seems that

both of the magnetic measurement for the 128 angular points and this data reduction give sufficient resolution, at least up to the 20-pole components, for the case without the experimental errors.

3.2 Results of Data Analysis

3.2.1 Helical Multipole Contents at 200 A

The multipole contents measured by 5 windings, dipole #1, dipole #2, tangential, quadrupole #1, and quadrupole #2, at I = 199.98 A on the increasing portion of the coil current are listed in Tables 3 - 7, respectively. On the estimation of the multipole contents from the measurements with the quadrupole windings, the reference field, $B_{ref}(k)$, estimated from the dipole #1 winding is utilized. For a comparison, the analytically calculated multipole coefficients for the case with the infinite permeability for the iron yoke, are also listed in Table 8.

Especially, the estimated normal sextupole coefficients, $b_3(k)$, are consistent among the measurements by 3 different windings, ranging from - 62 to - 63 $\times 10^{-4}$. The measured normal or skew decapole, 14 - pole, and 18 - pole are larger than the expected ones. This difference may happen from various errors of the rotating coil system, i.e., misalignment of pick-up coils, axis motion, and etc. [4,5] As the data have to be extrapolated to values for the reference radius $r_0 = 31$ mm, there is a possibility that the error of the higher multipole contents becomes larger.

3.2.2 Current Dependence of Helical Multiples

The current dependence of the helical reference field, $B_{ref}(k)$, and the multipole coefficients, $b_n(k)$ and $a_n(k)$, derived from the measurements with 5 pick-up coils, on the order of the experimental sequence, are plotted in Figs. 1 - 20, respectively. The results derived from the measurement with the dipole #1, the dipole #2, tangential, quadrupole #1, and quadrupole #2 winding are shown in Figs. 1 - 4, Figs. 5 - 8, Figs. 9 - 14, Figs. 15 - 17, and Figs. 18 - 20, respectively.

4 CONCLUSION

The multipole contents for the helical dipole prototype magnet are simply obtained without the elaborate correction from the data reduction of the magnetic measurement by the rotating coil, with some discrepancies among the derived values from the various pick-up coils. Then, it may be necessary to consider the experimental errors due to the geometrical imperfections of the pick-up coils as well as from a displacement and motion of the pick-up coil axis during rotation. [4,5]

5 ACKNOWLEDGMENTS

The author is indebted for providing the experimental data to R. Thomas and A. Jain, and for helpful discussions and comments to M. Okamura, E. Willen, and T. Katayama.

REFERENCES

[1] R. Thomas, Private communications.
[2] A. Jain, Private communications.
[3] T. Tominaka, "Expressions for the Magnetic Flux Enclosed by Rotating Coils in Helical Dipoles", AGS/RHIC/SN to be published.
[4] R. Meinke, P. Schmüser and Y. Zao, "Methods of Harmonic Measurements in the Superconducting HERA Magnets and Analysis of Systematic Errors", DESY report HERA 91 - 13 (1991).
[5] K. -H. Mess, P. Schmüser and S. Wolff, "Superconducting Accelerator Magnets", World Scientific, pp.181 - 188 (1996).

Table 2 Check of analysis method for data measured with tangential winding.

n (Bref) [T]	Pole	bn-f.a. 4.	an-f.a.	bn-spec. 4.	an-spec.
1	dipole	1.	5.421×10^{-10}	1.	0
2	quadrupole	0.001	-0.0002	0.001	-0.0002
3	sextupole	0.0009	-0.0002	0.0009	-0.0002
4	octupole	0.0008	0.0002	0.0008	0.0002
5	decapole	0.0007	0.0002	0.0007	0.0002
6	dodecapole	0.0006	-0.0001	0.0006	-0.0001
7	14-pole	0.0005	-0.0001	0.0005	-0.0001
8	16-pole	0.0004	0.0001	0.0004	0.0001
9	18-pole	0.0003	0.0001	0.0003	0.0001
10	20-pole	0.0001998	-0.00005014	0.0002	-0.00005

Table 3 Measured helical normal and skew multipole coefficients derived from the measurement with rotaing coil (dipole winding #1), with r0=31 mm, at I=199.98 A.

n (Bref) [T]	Pole	bn-meas. 2.713	an-meas.
1	dipole	1.	5.017×10^{-17}
2	quadrupole	?	?
3	sextupole	-0.006337	0.0001531
4	octupole	?	?
5	decapole	0.001651	0.0002511
6	dodecapole	?	?
7	14-pole	-0.002823	-0.0008514
8	16-pole	?	?
9	18-pole	-0.002452	-0.004565
10	20-pole	?	?

Table 4 Measured helical normal and skew multipole coefficients derived from the measurement with rotaing coil (dipole winding #2), with r0=31 mm, at I=199.98 A.

n (Bref) [T]	Pole	bn-meas. 2.714	an-meas.
1	dipole	1.	3.825×10^{-16}
2	quadrupole	?	?
3	sextupole	-0.006232	-0.0002485
4	octupole	?	?
5	decapole	-0.0003239	0.001597
6	dodecapole	?	?
7	14-pole	0.002656	-0.003427
8	16-pole	?	?
9	18-pole	-0.0004404	0.005803
10	20-pole	?	?

Table 5 Measured helical normal and skew multipole coefficients derived from the measurement with rotaing coil (tangential winding), with r0=31 mm, at I=199.98 A.

n	Pole	bn-meas.	an-meas.
(Bref) [T]		2.721	
1	dipole	1.	9.998×10^{-17}
2	quadrupole	0.0001157	-0.0000407
3	sextupole	-0.006317	-0.00002602
4	octupole	0.0002265	2.752×10^{-6}
5	decapole	0.0009713	0.0002434
6	dodecapole	-0.00005385	-0.0001217
7	14-pole	0.0003346	0.0007271
8	16-pole	0.00005085	-0.0004008
9	18-pole	-0.001967	0.0001566
10	20-pole	0.002047	0.0006874

Table 6 Measured helical normal and skew multipole coefficients derived from the measurement with rotaing coil (quadrupole winding #1), with r0=31 mm, at I=199.98 A, with the assumption of Bref=2.713 T and a2=0.

n	Pole	bn-meas.	an-meas.
(Bref) [T]		2.713	
2	quadrupole	0.00006586	-3.49×10^{-19}
6	dodecapole	0.00003524	-0.00003798
10	20-pole	-0.0002408	-0.00008336

Table 7 Measured helical normal and skew multipole coefficients derived from the measurement with rotaing coil (quadrupole winding #2), with r0=31 mm, at I=199.98 A, with the assumption of Bref=2.713 T and a2=0.

n	Pole	bn-meas.	an-meas.
(Bref) [T]		2.713	
2	quadrupole	0.00005217	7.31×10^{-20}
6	dodecapole	0.00002449	-0.00002045
10	20-pole	-0.0007237	-0.0004239

Table 8 Analytically calculated helical multipole coefficients, with r0=31 mm, at I=200 A, for the case of the iron yoke with the infinite permeability.

n	Pole	bn-ana.
(Bref) [T]		2.809
1	dipole	1.
3	sextupole	-0.004926
5	decapole	0.0005491
7	14-pole	0.00002848
9	18-pole	-0.0007564

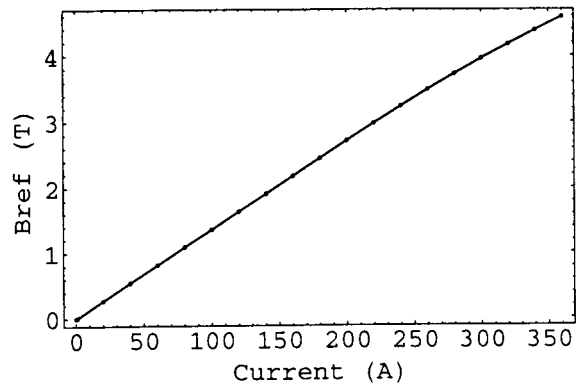

Fig.1 Dipole field, Bref v.s. current, derived from the measurement with dipole winding #1.

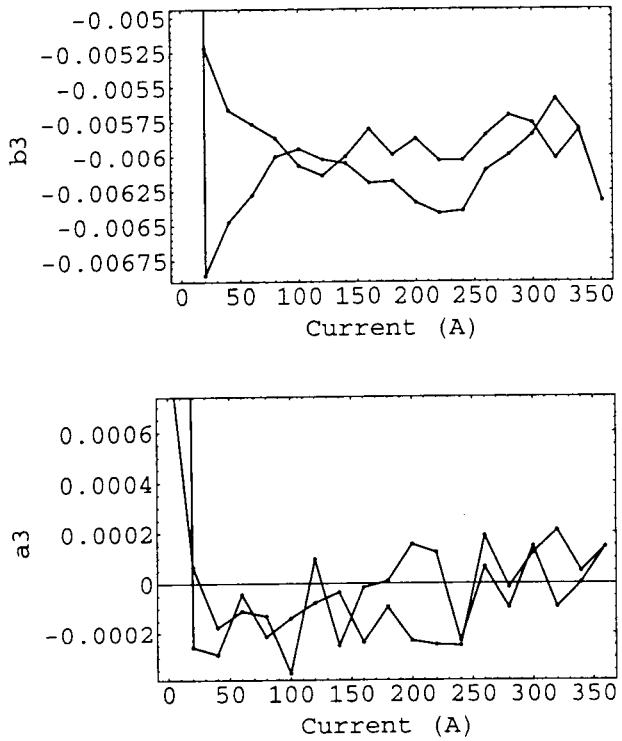

Fig.2 Sextupole coefficients, b3 (normal) and a3 (skew) v.s. current, derived from the measurement with dipole winding #1.

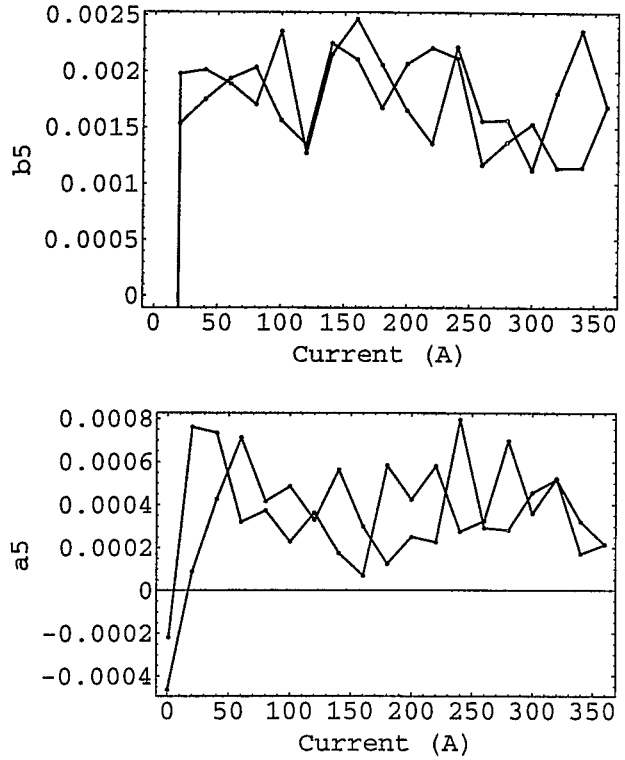

Fig.3 Decapole coefficients, b5 (normal) and a5 (skew) v.s. current, derived from the measurement with dipole winding #1.

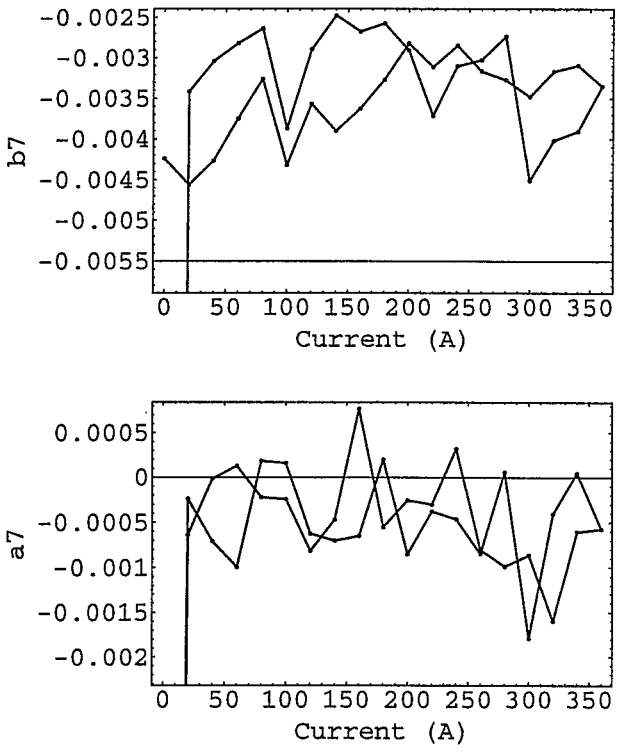

Fig.4 14-pole coefficients, b7 (normal) and a7 (skew) v.s. current, derived from the measurement with dipole winding #1.

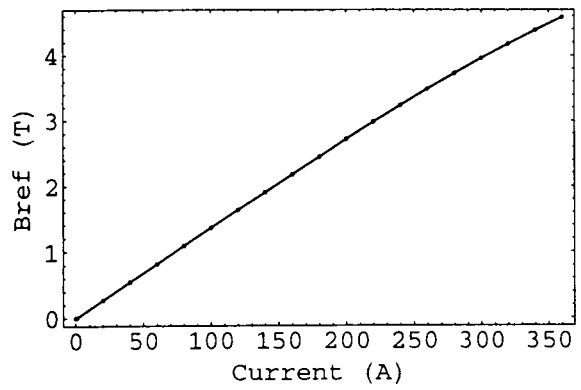

Fig.5 Dipole field, Bref v.s. current, derived from the measurement with dipole winding #2.

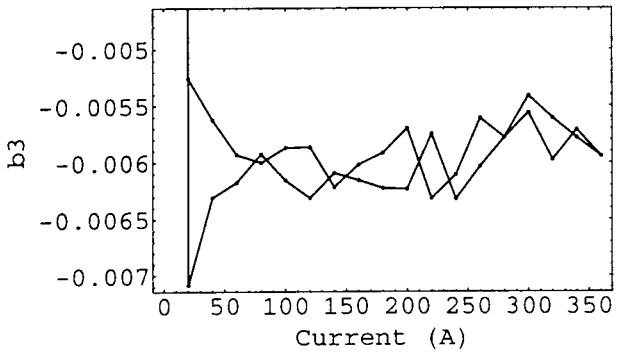

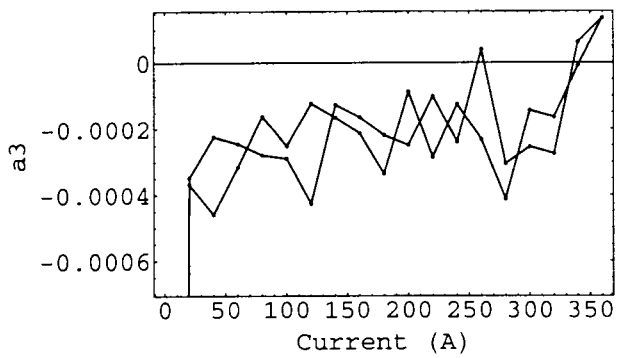

Fig.6 Sextupole coefficients, b3 (normal) and a3 (skew) v.s. current, derived from the measurement with dipole winding #2.

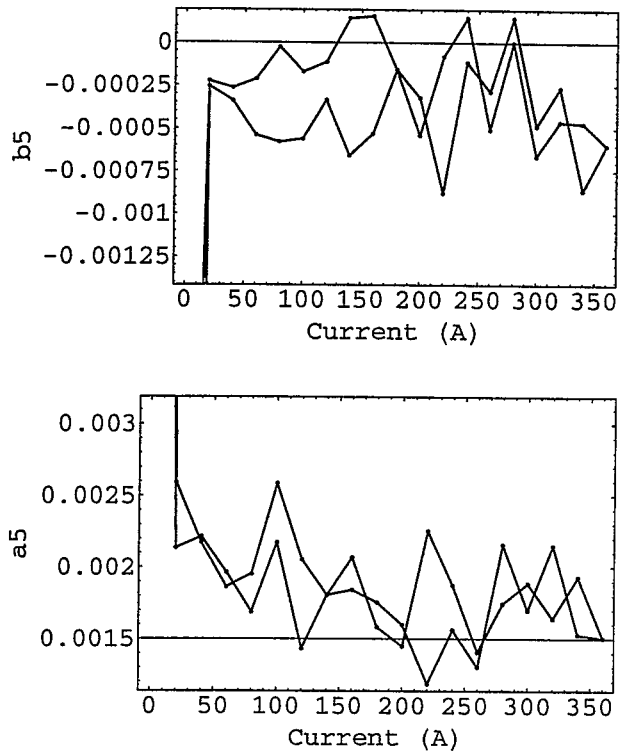

Fig.7 Decapole coefficients, b5 (normal) and a5 (skew) v.s. current, derived from the measurement with dipole winding #2.

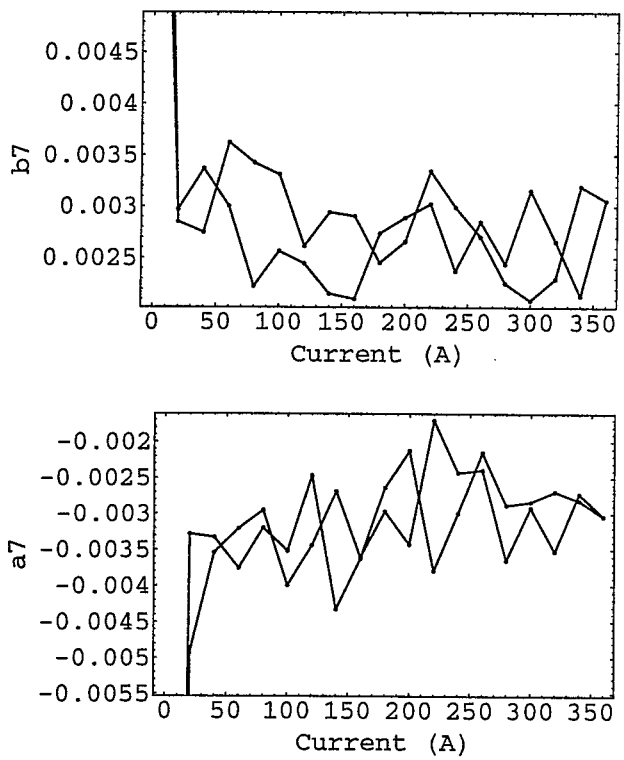

Fig.8 14-pole coefficients, b7 (normal) and a7 (skew) v.s. current, derived from the measurement with dipole winding #2.

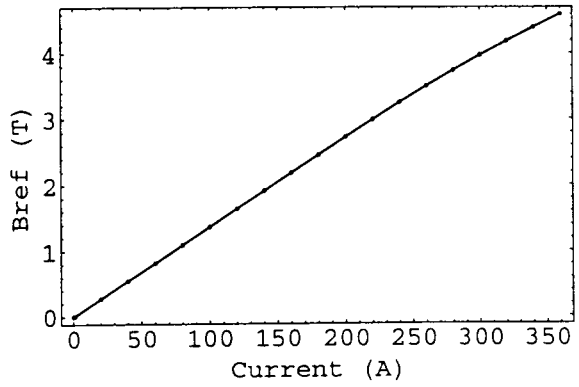

Fig.9 Dipole field, Bref v.s. current, derived from the measurement with tangential winding.

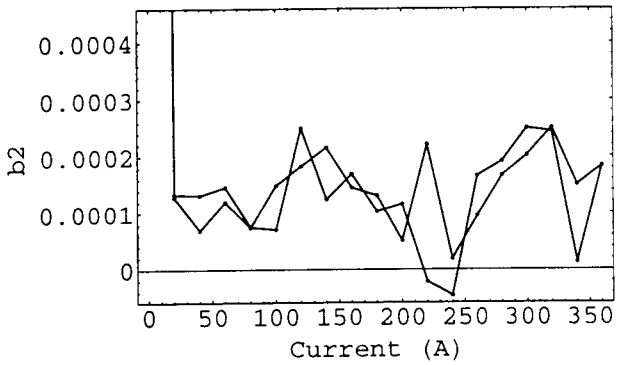

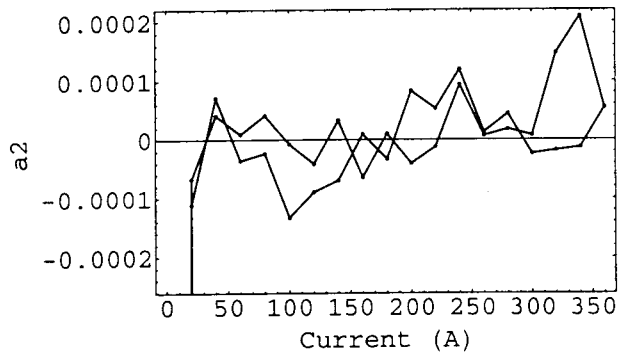

Fig.10 Quadrupole coefficients, b2 (normal) and a2 (skew) v.s. current, derived from the measurement with tangential winding.

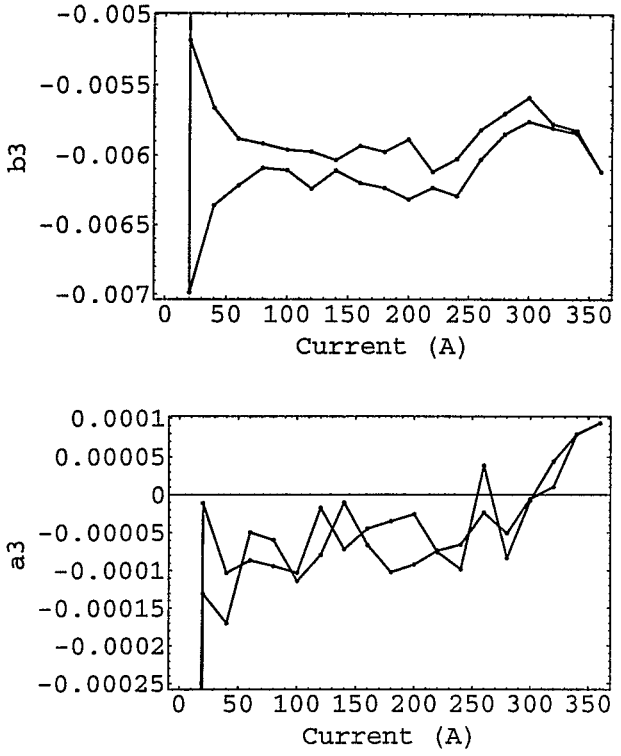

Fig.11 Sextupole coefficients, b3 (normal) and a3 (skew) v.s. current, derived from the measurement with tangential winding.

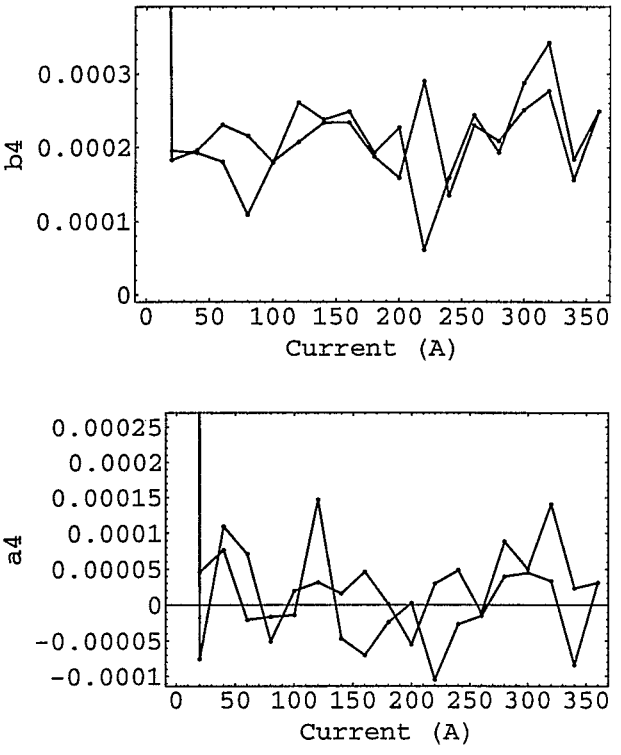

Fig.12 Octupole coefficients, b4 (normal) and a4 (skew) v.s. current, derived from the measurement with tangential winding.

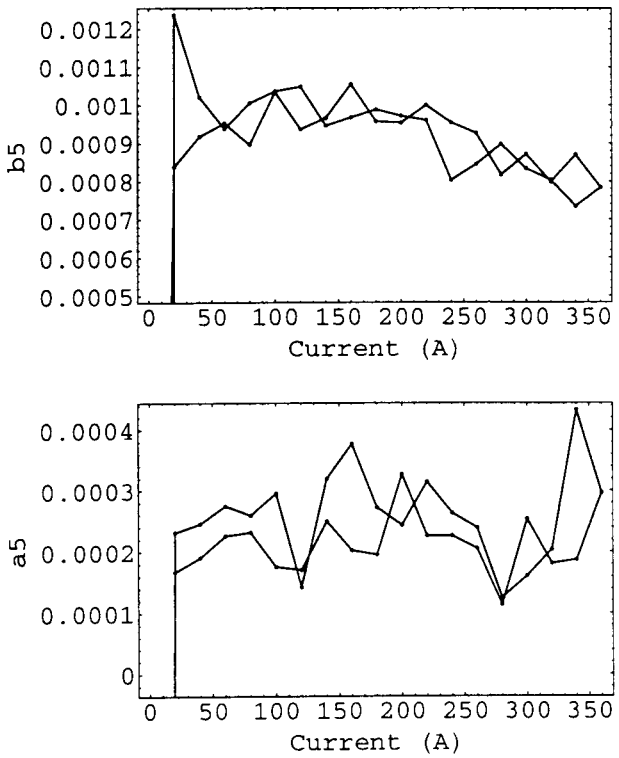

Fig.13 Decapole coefficients, b5 (normal) and a5 (skew) v.s. current, derived from the measurement with tangential winding.

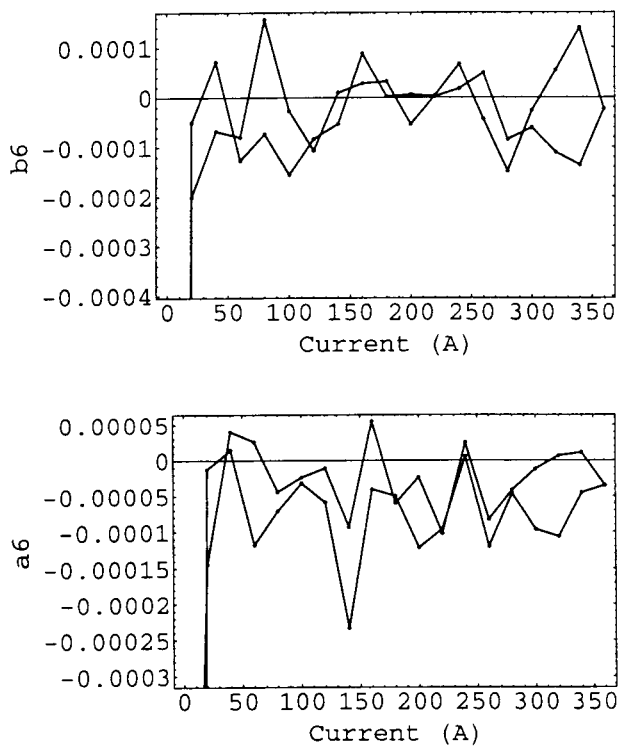

Fig.14 Dodecapole coefficients, b6 (normal) and a6 (skew) v.s. current, derived from the measurement with tangential winding.

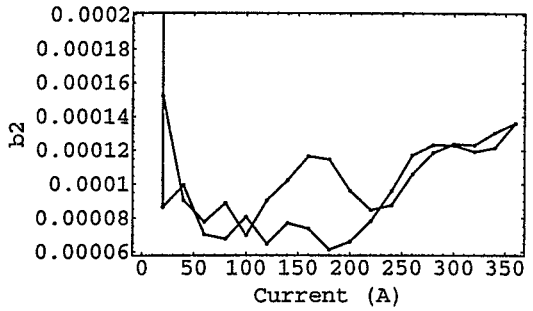

Fig.15 Quadrupole coefficient, b2 (normal) v.s. current, with a2=0, derived from the measurement with quadrupole winding #1.

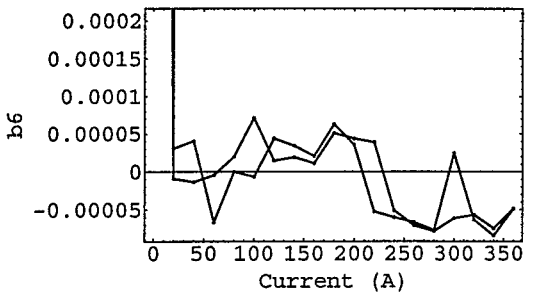

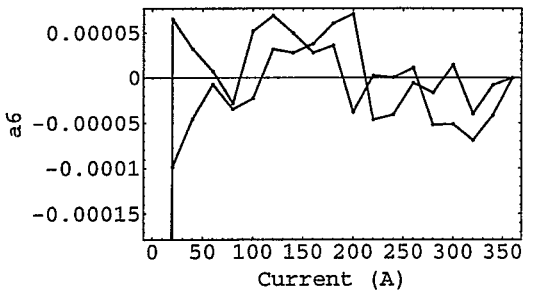

Fig.16 Dodecapole coefficients, b6 (normal) and a6 (skew) v.s. current, derived from the measurement with quadrupole winding #1.

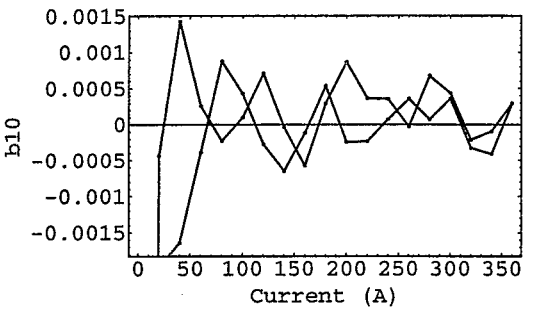

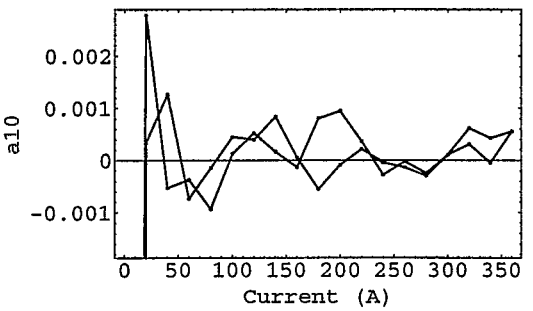

Fig.17 20-pole coefficients, b10 (normal) and a10 (skew) v.s. current, derived from the measurement with quadrupole winding #1.

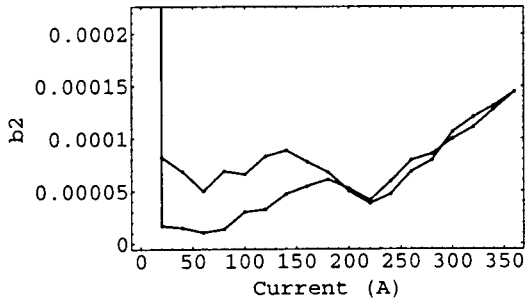

Fig.18 Quadrupole coefficient, b2 (normal) v.s. current, with a2=0, derived from the measurement with quadrupole winding #2.

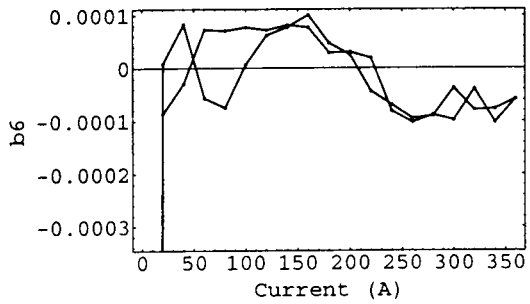

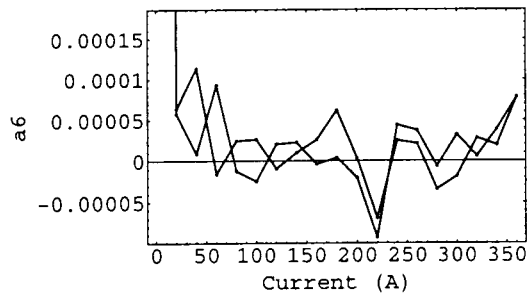

Fig.19 Dodecapole coefficients, b6 (normal) and a6 (skew) v.s. current, derived from the measurement with quadrupole winding #2.

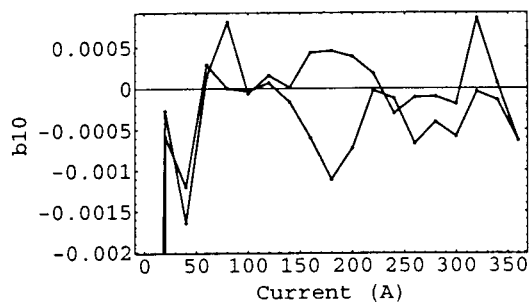

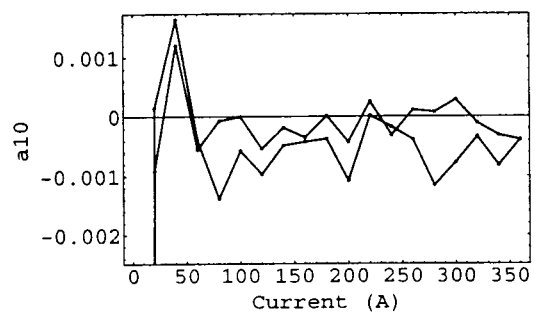

Fig.20 20-pole coefficients, b10 (normal) and a10 (skew) v.s. current, derived from the measurement with quadrupole winding #2.